Journal of Fluorescence, Vol. 2, No. 1, 1992

LL-Dityrosine: A Time-Resolved Fluorescence Investigation

Andreas J. Kungl,[1,5] Gerhard Landl,[2] Antonie J. W. G. Visser,[3] Michael Breitenbach,[4] and Harald F. Kauffmann[1]

Received February 21, 1992; revised June 3, 1992; accepted June 4, 1992

We have investigated the time-resolved fluorescence properties of LL-dityrosine in aqueous solution. Typically, three exponential components were needed to fit the fluorescence pattern adequately, with pure decay terms for the low-intensity, high-energy state (λ_{em} = 350 nm) but with a pronounced subnanosecond rise phase for the predominant red-edge fluorescence (λ_{em} > 380 nm, λ_{max} = 408 nm). Dual fluorescence behavior is indicative of an intramolecular precursor–successor pair, i.e., a consecutive intramolecular excited-state reaction. We suggest that this reaction is a torsional motion of the (deprotonated) monoanion along the biphenolic bond. Analysis of the fluorescence anisotropy decay of dityrosine yielded two rotational correlation times, the longer of which is associated with a negative preexponential term. The increase with time in the horizontally polarized component of the intensity decay is interpreted as the result of an electronic rearrangement in the excited state when the successor form of dityrosine is generated. Lifetime distributions of experimental data were probed by an unbiased exponential series method which uses a Tikhonov-type regularization function. The procedure revealed three well-separated groups of lifetimes, the short-lived ensemble forming a formally negative distribution. A photophysical model is introduced which interprets the biexponential decay of dityrosine in terms of overlapping emission signals from the precursor and the successor molecule.

KEY WORDS: Dityrosine; excited-state reaction; distributional analysis; fluorescence anisotropy decay.

INTRODUCTION

There has been a great deal of interest over the past decade in using fluorescence methods to study biological materials [1,2]. Time-resolved fluorescence techniques have been applied to probe excited-state relaxation of aromatic amino acids such as tryptophan [3–5] and tyrosine [6,7], conformational dynamics of tryptophan-containing proteins [8,9], and excitation energy transport in photosynthesis [10].

An important question extensively addressed in the literature has been the mechanistic interpretation of fluorescence relaxation patterns of biomolecules in solution. There is evidence now from a large set of experimental data that the fluorescence decay of individual amino acid residues in proteins is multiexponential and that even single amino acids freely diffusing in water display a pronounced deviation from monoexponential decay. In particular, the question of multiple lifetime fluorescence exhibited by indole and its derivatives has received considerable attention in the past (for re-

[1] Institut für Physikalische Chemie der Universität Wien, Währingerstraße 42, A-1090 Wien, Austria.
[2] Institut für Mathematik, Johannes-Kepler-Universität, A-4040 Linz, Austria.
[3] Department of Biochemistry, Agricultural University, Dreijenlaan 3, NL-6703 HA Wageningen, The Netherlands.
[4] Abteilung für Genetik und Entwicklungsbiologie, Universität Salzburg, Hellbrunnerstraße 34, A-5020 Salzburg, Austria.
[5] To whom correspondence should be addressed at Max-Planck-Institut für Biochemie, Abt. Strukturforschung, Am Klopferspitz, DW-8033 Martinsried, FRG.

1053-0509/92/0300-0063$06.50/0

view see Ref. 11). Currently popular concepts have correlated the number of exponentials to the number of excited-state conformers in linear kinetic schemes [3,12]. Special emphasis has been given to the C_α–C_β (χ_1) rotamers of tryptophan, the conformation of which generates different orientations of the indole-ring relative to the amino and the carboxyl group of the alanyl side chain. These specific conformations yield different rates of charge-transfer quenching in the excited state and, thus, different lifetimes with amplitudes related to the ground-state conformers of tryptophan. The so-called rotamer model has been extended to include solvation and solvent relaxation in the decay process [13]. Strong evidence in favor of the conformer hypothesis has been found by ^{1}H-NMR spectroscopy of tyrosine [7], and further support to the model has been given by supersonic jet-expansion experiments of tryptophan both in the absence [14] and in the presence of stabilizing solvent effects [15].

However, for systems of increasing complexity (e.g., proteins), the dispersion of fluorescence brought about by a distribution of conformational states must show up in a pronounced nonexponential behavior, thus revealing the limits of a free-fit, multiexponential reconvolution procedure. In this situation, the number of extractable exponentials must be considered to be the result of a curve parametrization only, which conceals the underlying distribution [16–18]. Up to now, nonexponentiality of protein fluorescence due to a distribution of event times has been the subject of experimental and numerical work. Trial probability functions modeled for frequencies of interconversion between conformational states [19] as well as for distance fluctuations in energy transfer [20] have been implemented in frequency-domain fluorescence data analysis and distribution parameters have been evaluated by means of an iterative fit-and-compare nonlinear least-squares algorithm. Very recently, methods have been developed that avoid specific distribution functions but, rather, deconvolute the fluorescence data by an unbiased algorithm to obtain the unknown shapes of distributions. The exponential series method (ESM) developed by James and Ware [16] has become an effective tool for mapping out distributed event times for high-precision, high-resolution single-photon counting data [18]. In addition, the method of entropy maximization [21] adapted to time-domain fluorescence analysis by Livesey and Brochon [22] has proved useful in the reconstruction of lifetime patterns from complex protein fluorescence decays [9,23].

LL-Dityrosine (Fig. 1) is the product of the oxidative reaction between L-tyrosine and H_2O_2 catalyzed by peroxidase *in vitro* [24]. The proposed structure was recently shown to be correct by a ^{13}C-NMR spectroscopic investigation [25]. The biphenolic bond was shown to be located *ortho,ortho* to the hydroxyl groups (Fig. 1). LL-Dityrosine was found to be a constituent of acid hydrolysates of a number of biological materials such as insect cuticular resilin [26], tussah silk fibroin [27], the spore coat of *Bacillus subtilis* [28], the fertilization membrane of the sea urchin egg [29], and the outermost layer of the ascospore wall of the yeast *Saccharomyces cerevisiae* [25,30]. Furthermore, dityrosine is produced by exposing proteins to ionizing radiation [31]. In all these systems, dityrosine was detected by its characteristic natural fluorescence. Invariably, it is a component of insoluble materials with structural features. Therefore, it has been suggested that dityrosine forms covalent protein–protein cross-links *in vivo*. Probably, these are made postsynthetically via a peroxidative reaction in order to aid the mechanical stability of the particular biological structure. Such a cross-linking reaction was first observed *in vitro* with horseradish peroxidase [32]. However, final proof for this function of dityrosine *in vivo* is still missing. Little is known about the biochemical pathway of dityrosine biosynthesis in various organisms. Only in the fertilized sea urchin egg has a peroxidase been characterized with the major function of dityrosine formation [33].

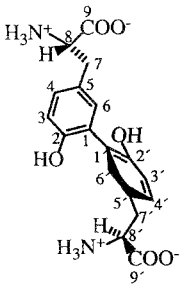

Fig. 1. Structure of LL-dityrosine.

We want to present here a detailed picture of the fluorescence behavior of dityrosine under varying pH conditions. To our knowledge, no transient fluorescence studies have been reported for dityrosine in solution so far (the work of Small and Anderson [34] regarding the fluorescence of dityrosine in a protein is discussed). We report here on a dual-fluorescence system that, in our interpretation, is caused by an intramolecular precursor–successor pair in the excited state. Some efforts are made to rationalize the kinetic background of the proposed reaction in the excited state and its mechanistic pathway. In addition, to discuss the fluorescence data also in terms of distributions, a modified exponential series algorithm,

ESM, has been used [35] in this work which is sufficiently stable in rise phase analysis, thus allowing even negative amplitudes to be resolved in a free-parameter optimization.

MATERIALS AND METHODS

LL-Dityrosine was synthesized by oxidation of L-tyrosine (Sigma) with horseradish peroxidase (Sigma) according to Amado *et al.* [32] and purified on a DEAE column developed with a linear gradient of 0.02 *M* Na_2HPO_4 and 0.06 *M* NaH_2PO_4 followed by a Sephadex G-10 column chromatography according to Andersen [36] (buffers were freshly prepared before use). This was followed by HPLC purification on a Polygosil C_{18} column (250 × 16 mm, 10 μm) using a Waters Delta Prep 3000 HPLC system. The column was developed with a gradient of CH_3CN in 0.01 *M* trifluoroacetic acid (0–15% CH_3CN in 40 min); the flow rate was 8 ml/min.

Dityrosine was detected by measuring the absorption at 280 nm. Trifluoroacetic acid was removed by rotary evaporation. The residue was taken up in 2 ml of H_2O, yielding a concentration of 5.95×10^{-3} mol/L ($\epsilon_{320\,nm} = 12{,}900 \pm 1500\ cm^{-1}M^{-1}$). For fluorescence measurements the solution was diluted with freshly prepared 2×10^{-3} *M* ammonium acetate or sodium phosphate buffer to a final concentration of 6×10^{-5} *M*. For adjusting the pH, aqueous solutions of ammonia and HCl were used and monitored on a Metrohm 632 pH-meter.

Steady-state fluorescence and fluorescence excitation spectra were collected on a Hitachi Perkin–Elmer MPF 4 spectrometer. The excitation wavelength of dityrosine fluorescence ranged from 285 to 320 nm, depending on the pH of the solution. In general, slits giving bandwidths of 2–4 nm were used. Fluorescence excitation spectra of dityrosine were monitored at wavelengths λ_{em} = 380–450 nm. Spectra presented in this study are uncorrected.

Time-resolved fluorescence was performed on a serial PRA 3000 transient configuration (Photochemical Research Associates Inc., Canada) using a thyratron-gated hydrogen flash lamp. The full width at half-maximum (FWHM) of the lamp instrumental function *L(t)* was typically 1.5 ns. Fluorescence photons were detected by a Hamamatsu R928 photomultiplier and time-correlated by single-photon timing [37]. TAC-processed output signals were collected in a Tracor Northern TN 1750 multichannel analyzer and the fluorescence histogram was then transferred to a MicroVAX II for data accomodation. No significant nonlinearities in the TAC were detected. Instrumental response functions were collected both at the excitation wavelength (λ_{ex} = 285/320 nm) and at the emission wavelength (λ_{em} = 408 nm) to rule out an energy-dependent delay (photomultiplier color effect) extractable as an artificial short-time exponential in numerical rise phase analysis (Table I).

Two methods of data analysis were used in this work. First, fluorescence raw data *H(t)* were analyzed by the usual nonlinear least-squares reconvolution technique [38]

$$H(t) = L(t) \otimes F(t) \tag{1}$$

where the molecular δ-pulse fluorescence, *F(t)*, is assumed to be a sum of up to four discrete exponentials with both the amplitudes and the lifetimes floating in a free-fit procedure (PRA program FLUOR). In addition, a minimization program combining a Gauss–Newton and a quasi-Newton nonlinear regression algorithm was applied to fluorescence data analysis. Since none of the data sets could be fitted from the first channel of fluorescence intensity without getting for χ^2 a large deviation from 1 (rise phase), the sum of the experimental amplitudes in Table I does not equal zero in every case, as theoretically predicted.

Second, for the evaluation of a potential distribution of fluorescence lifetimes from a (nonexponential) δ-pulse fluorescence response,

$$F(t) = \int_0^\infty a(\tau)\exp(-t/\tau)d\tau \tag{2}$$

a modified exponential series method (ESM) developed in this laboratory [35] was used in raw data analysis. In the ESM, *F(t)* in Eq. (2) is approximated by a coarse discretization. By using terms of a series of exponentials with fixed lifetimes τ_n (equally or logarithmically spaced over the time scale of fluorescence), the method, in principle, allows the corresponding discrete set of amplitudes $\{a_n\}$ to be evaluated from the convolution integral [Eq. (1)] in a linear, least-squares free-parameter optimization.

Our ESM uses a hybrid-algorithm similar to that of Al-Baali and Fletcher [39], thus combining a Newton and a quasi-Newton method in such a way that the algorithm becomes—despite the ill-posedness of the Laplace inversion in Eq. (2)—"as stable as possible" [35]. In general, our ESM is robust and it works well on synthetic and high-accuracy real data. There is no cutoff required for deleting amplitudes of values close to zero during the reconvolution, and contrary to other exponential series techniques, our method is not restricted to positive amplitudes (pure decays). Negative values for the amplitudes (rise phase) are also possible. In all cases,

Table I. Multiexponential Reconvolution Parameters of Dityrosine Fluorescence Decay at Different pH's and Various Emission Wavelengths[a]

pH	λ_{ex}(nm)	λ_{em}(nm)	B_1	B_2	B_3	T_1	T_2	T_3	χ^2
0.98	284	408	−1.18 ± 0.13	0.38 ± 0.06	0.48 ± 0.01	0.16 ± 0.04	0.80 ± 0.09	2.43 ± 0.01	1.31
2.07	284	406	−0.64 ± 0.10	0.19 ± 0.13	0.37 ± 0.008	0.29 ± 0.06	0.81 ± 0.25	2.82 ± 0.19	1.21
3.01	284	408	−0.54 ± 0.03	0.10 ± 0.01	0.32 ± 0.006	0.22 ± 0.03	1.26 ± 0.22	3.76 ± 0.02	1.25
4.09	283	408	−0.73 ± 0.15	0.19 ± 0.06	0.46 ± 0.06	0.15 ± 0.03	2.91 ± 0.36	4.59 ± 0.11	0.92
5.08	285	407	−0.52 ± 0.11	0.14 ± 0.005	0.25 ± 0.007	0.13 ± 0.03	1.99 ± 0.12	4.51 ± 0.03	1.11
5.80	285	408	−0.51 ± 0.05	0.10 ± 0.005	0.27 ± 0.004	0.15 ± 0.02	1.68 ± 0.13	4.53 ± 0.02	1.04
6.94	317	408	−0.56 ± 0.08	0.15 ± 0.10	0.34 ± 0.002	0.29 ± 0.05	0.82 ± 0.21	4.58 ± 0.01	0.94
8.23	319	408	−0.42 ± 0.01	0.06 ± 0.01	0.28 ± 0.002	0.23 ± 0.03	1.23 ± 0.25	4.58 ± 0.01	1.16
9.07	320	407	−0.73 ± 0.02	0.22 ± 0.02	1.01 ± 0.01	0.29 ± 0.03	1.55 ± 0.16	4.62 ± 0.01	1.21
10.0	317	410	−0.45 ± 0.04	0.05 ± 0.007	0.34 ± 0.004	0.16 ± 0.02	1.64 ± 0.26	4.75 ± 0.02	1.05
4.80	285	350	$1.36^{(*)}$ ± 0.05	$0.02^{(*)}$ ± 0.004	$0.04^{(*)}$ ± 0.003	0.20 ± 0.01	1.70 ± 0.47	4.29 ± 0.09	1.01
4.80	285	390	−0.10 ± 0.03	0.07 ± 0.04	0.19 ± 0.002	0.40 ± 0.19	1.13 ± 0.29	4.15 ± 0.02	0.92
4.80	285	408	−0.30 ± 0.02	0.11 ± 0.005	0.20 ± 0.006	0.23 ± 0.03	1.84 ± 0.14	4.45 ± 0.03	1.20
4.80	285	450	−0.21 ± 0.07	0.17 ± 0.08	0.24 ± 0.004	0.44 ± 0.17	1.12 ± 0.23	4.16 ± 0.02	0.99

[a] T_i, lifetime values; B_i, preexponentials according to Eq. (1). Values with a superscript asterisk refer to amplitudes A_i, according to Eq. (2) (pure decay). The fluorescence parameters presented are unaffected by the choice of the analyzing fluorescence wavelength in the low-energy regime of the dityrosine spectrum. Thus, for transient runs done at emission wavelengths in the range 390–480 nm of the steady-state fluorescence spectrum (Fig. 2, curve d), no changes occur in the number of exponentials or in the values of the time constants and amplitudes.

a rectangular distribution of start parameters was applied in the ESM probe function in order to avoid a preconceived bias in the computation. Generally, 70 lifetimes were set in the analysis. Details of the method are given elsewhere [35].

Time-resolved fluorescence anisotropy experiments were obtained as described earlier [40,41]. An argon ion laser (Coherent Radiation CR18) was mode-locked and a DCM dye laser (modified CR590) was synchronously pumped and frequency doubled to have 340-nm radiation. To decrease the 76-MHz repetition rate of exciting light pulses to 596 kHz, an electrooptic modulator setup was used [42]. The energy of exciting light pulses was in the subnanojoule region. A Baird Atomic 402.3-nm interference filter was combined with a KV389 cutoff filter (Schott) to select fluorescence emission and a fast 90° rotating sheet polarizer (Polaroid) was used to select emission polarized vertically or horizontally with respect to the polarization direction of the excitation light. Fluorescence photons were detected using a Hamamatsu R1645U-01 microchannel plate detector and further processed by time-correlated single-photon counting. In two subgroups (1024 channels each) of the memory of a multichannel analyzer (Nuclear Data ND66), semisimultanously recorded data of vertically and horizontally polarized fluorescence were collected. A reference compound with a fluorescence lifetime of a few picoseconds [43] was measured before and after the fluorescence experiment and the average of the two was taken in the deconvolution procedure. Data analysis was performed as detailed by Vos *et al.* [44] or with the software from Globals Unlimited (Urbana, Illinois).

RESULTS

In Figs. 2 and 3 the steady-state spectra of aqueous dityrosine (6×10^{-5} *M*) are given. Curves a, b, and c in Fig. 2 show the fluorescence excitation spectra (λ_{em} = 408 nm) at varying pH values: pH 2.0 (a), 6.94 (b), and 10,0 (c), respectively. The spectra are very similar to the absorption spectra (Fig. 3). The slight distortion in the intensity ratio of the two peaks in the excitation spectrum (curve b, Fig. 2) is probably due to a small reabsorption effect or to the fact that the spectra are not completely corrected. No dependence of the excitation spectra on the emission wavelength was found, thus demonstrating the high spectral purity of the compound. A prominent feature of the excitation (absorption) spectra is the pronounced shift of the peak maximum from 285 to 320 nm on varying the pH from the acidic to the basic medium. This is the result of a specific ground-state deprotonation of one of the phenolic hydroxyl groups (Fig. 1). However, the bathochromic shift of 35 nm is unusually large, so one would expect an additional ground-state stabilization in the basic medium that may be caused by a partial delocalization of the lone-pair electrons of the deprotonated oxygen into the aromatic ring system (see Discussion). Accordingly, the spectrum at pH 6.94 (curve b, Fig. 2) is a superposition of two contributions

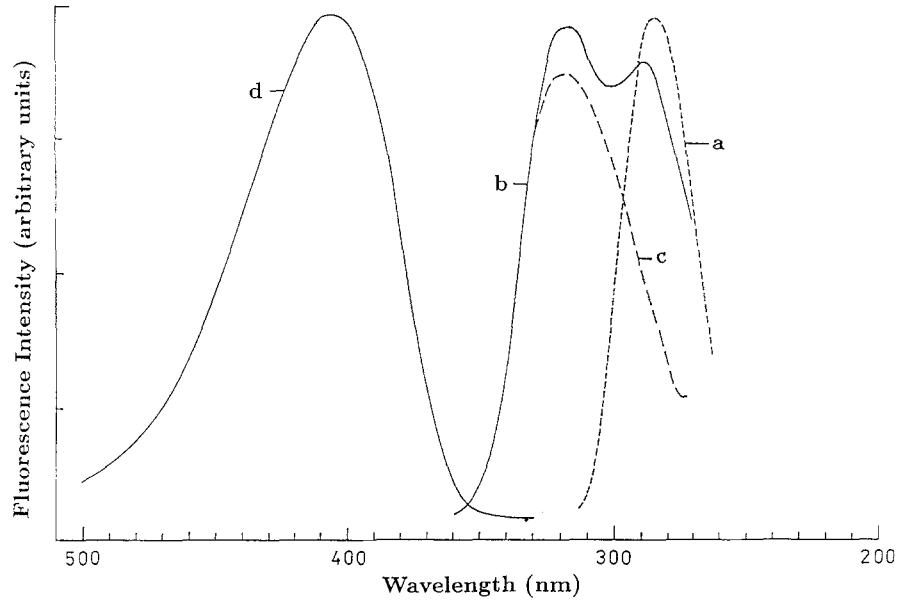

Fig. 2. Photostationary spectra of LL-dityrosine in aqueous solution (6×10^{-5} *M*, *T* = 20°C). Curves a, b, and c: fluorescence excitation spectra (λ_{em} = 408 nm) at pH 2.0, 6.94, and 10.0, respectively. Curve d: total fluorescence spectrum. See the text for further details.

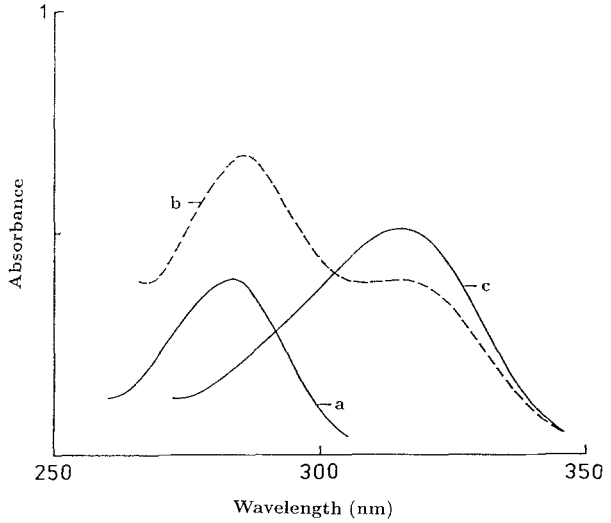

Fig. 3. Absorption spectra of LL-dityrosine in aqueous solution (6×10^{-5} *M*, *T* = 20°C). Curves a, b, and c: absorbance at pH 2.0, 6.94, and 10.0, respectively.

resulting from excitation of both the protonated and the deprotonated form.

Curve d in Fig. 2 shows the fluorescence spectrum, which, in contrast to the excitation (absorption) spectra, is unaffected by the pH of the solution. This suggests that the fluorescent state of dityrosine is independent of the ionization of the ground state. A further central issue is that the fluorescence is subject to a large Stokes' shift with an emission maximum at 408 nm. The obvious interpretation is that the emitting state of dityrosine is not identical to its vertically excited state. The low-energy emitting state is indicative of a system of considerable stability. It is tempting to hypothesize that the emissive species is the result of a consecutive reaction in the excited state leading to a molecular transformation of the primary Frank-Condon state of dityrosine.

The sequential nature of the dityrosine fluorescence for emission wavelengths $\lambda_{em} > 380$ nm is clearly demonstrated by time-resolved measurements. Figure 4 shows a typical transient fluorescence profile of dityrosine collected near the intensity maximum at λ_{em} = 408 nm (pH 4.0). Multiexponential reconvolution analysis yields a best-fit triple-exponential form, according to

$$F_{408}(t) = B_1\exp[-t/T_1] + B_2\exp[-t/T_2] + B_3\exp[-t/T_3] \quad (3)$$

with a distinct rise phase (the amplitude B_1 is negative) on a subnanosecond time scale (time constant T_1) and a double-exponential decay (B_2 and B_3 are positive) on a nanosecond time scale (time constants T_2 and T_3; see Table I). Since the subnanosecond order of magnitude of the rise time T_1 is associated with a high-amplitude B_1, the rise parameters behave relatively stably toward a variation of the starting channel in the rising-edge fit-

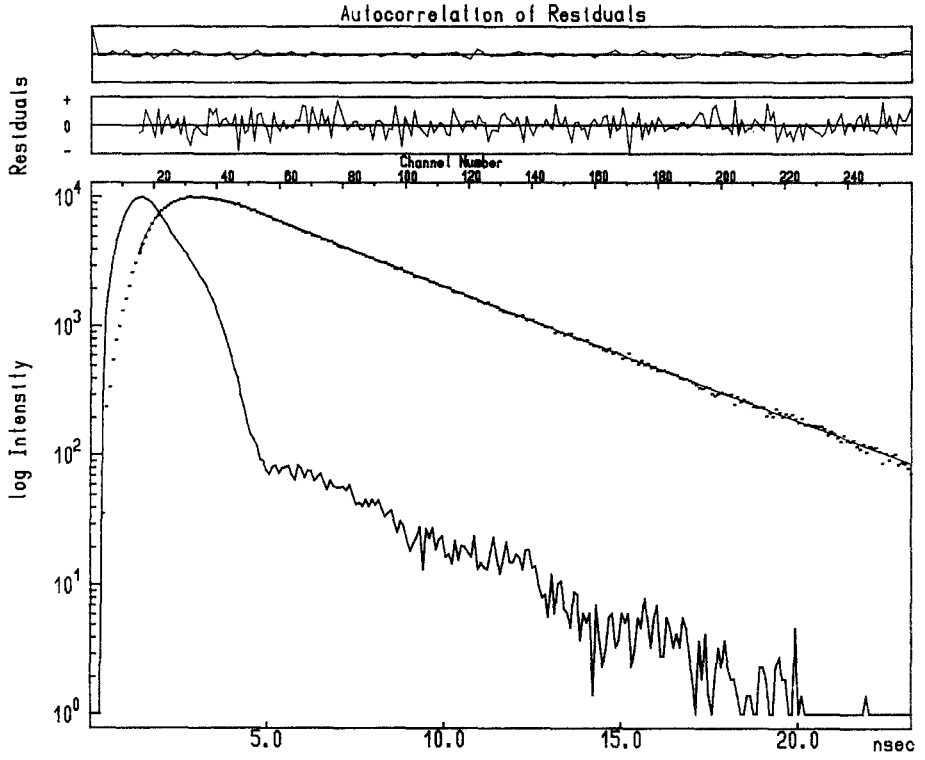

Fig. 4. Transient fluorescence of aqueous dityrosine at pH 4 and T = 20°C; data accumulated at λ_{em} = 408 nm and 0.1 ns/channel. Solid curve, lamp instrumental response; dots, experimental data; smooth solid line, best fit according to a triple-exponential form [Eq. (1) and Table I].

ting procedure. The rise term is, therefore, a substantial element of this analysis. Due to the relatively high-amplitude B_1 and the high data quality in this region, the rise term is a property of the system investigated, and not an artifact of numerical analysis. Consequently, all efforts to fit the experimental data to a bi- or triexponential term with rigorous constraints to positive amplitudes failed. This means that the fluorescent successor state of dityrosine is generated within approximately 200 ps (T_1 in Table I).

Considering only the decaying part in Fig. 4, the pure decay exhibits a pronounced departure from the monoexponential form and can be best approximated by a sum of two exponentials, even on larger time scales of relaxation. The results of fluorescence data fitting as a function of varying pH conditions are given in Table I. Table I contains the amplitudes, B_i, and the apparent lifetimes, T_i, of the transients. The values of B_i and T_i were optimized by the chi-square criterion from the free-fit multiexponential reconvolution. In general, parametrizations in terms of three exponentials were always required in order to fit the fluorescence patterns adequately in the pH range of 1–10. However, global analysis of data sets at different pH values failed the χ^2 criterion because of the difficulties that arise generally in rise-term analysis. The mean lifetime of the decay, $\langle\tau\rangle$, tends to be longer when the proton concentration is lowered. This fact is due mainly to T_3, which is significantly dependent on the pH of the solution. We suggest, therefore, that the H_3O^+ ion is an efficient quencher of the dityrosine fluorescence.

In order to reveal the Franck–Condon fluorescent state of dityrosine, transient fluorescence data were collected systematically by tuning the wavelength across the high-energy tail of dityrosine fluorescence, that is, the blue edge of the spectrum (λ_{em} = 350–370 nm). Indeed, a low-intensity fluorescence can be observed around λ_{em} = 350 nm that contains pure decay components, according to

$$F_{350}(t) = A_1\exp[-t/T_1] + A_2\exp[-t/T_2] + A_3\exp[-t/T_3] \quad (4)$$

with A_1 associated with a subnanosecond time constant which considerably exceeds A_2 and A_3 (Table I). We tentatively identify this emission to result from the proposed electronically excited precursor. However, con-

tribution of this precursor to the total fluorescence decreased with increasing emission wavelength (Table I, Fig. 5) and the amplitude A_1 changes its sign near 370 nm. To illustrate the effect of the emission wavelengths on the profiles of dityrosine fluorescence, an overlay representation of experimental data is given in Fig. 5. For clarity, the lamp profiles for curves b, c, and d have been omitted. This allows a better visual inspection of decay and rise processes at low channel numbers. The transients clearly show the heterogeneity of the emission band and the results suggest that, in particular, transient b is a superposition of two fluorescing states which are spectrally shifted relative to one another and, in our interpretation, represent the precursor and the successor states.

Next the time-resolved fluorescence spectra of dityrosine were analyzed to reveal underlying lifetime distributions. The ESM-recovered lifetime distribution from the dityrosine successor fluorescence at λ_{em} = 408 nm is presented in Fig. 6a. The shape of the graph is composed of a distribution of negative amplitudes in the short-lived domain (area A; centered at τ^c = 0.22 ns), a longer-lived distribution of positive amplitudes (area B; centered at τ^c = 0.9 ns), and a set of long-lived, positive amplitudes (area C; τ^c = 4.4 ns). In Fig. 6b the results of ESM obtained from the precursor fluorescence at λ_{em} = 350 nm are shown. Despite the low count rates in this spectral region, ESM analysis reveals a dominant distribution of positive amplitudes located at subnanosecond times with a central value τ^c = 0.3 ns. This distribution of short lifetimes in the precursor fluorescence agrees well with the shape, width, and central value of the rise-time distribution in the successor fluorescence (Fig. 6a). This indicates the photophysical correspondence of the precursor–successor pair. Some comments on the physical significance of distributional analysis in the case of the dityrosine fluorescence are given in the Discussion.

Measurements of the time-resolved fluorescence anisotropy were performed on a picosecond transient laser configuration. One thousand twenty-four channels were used, with 25.5 ps/channel, to cover the whole decay of dityrosine. In addition to the better time resolution compared to the PRA system, we were thus able to collect up to 10^5 counts in the peak channel maximum. The decay of the fluorescence anisotropy of dityrosine in water collected at λ_{em} = 402 nm (pH 10) is shown in Fig. 7. The anisotropy was calculated as the difference between convoluted parallel and perpendicular intensity components divided by the total convoluted fluorescence decay. For clarity, only the first 100 channels are shown in which all events take place. Also, the laser pulse and the total fluorescence, normalized to 0.5, are given in Fig. 7. The striking feature of this spectrum is that the

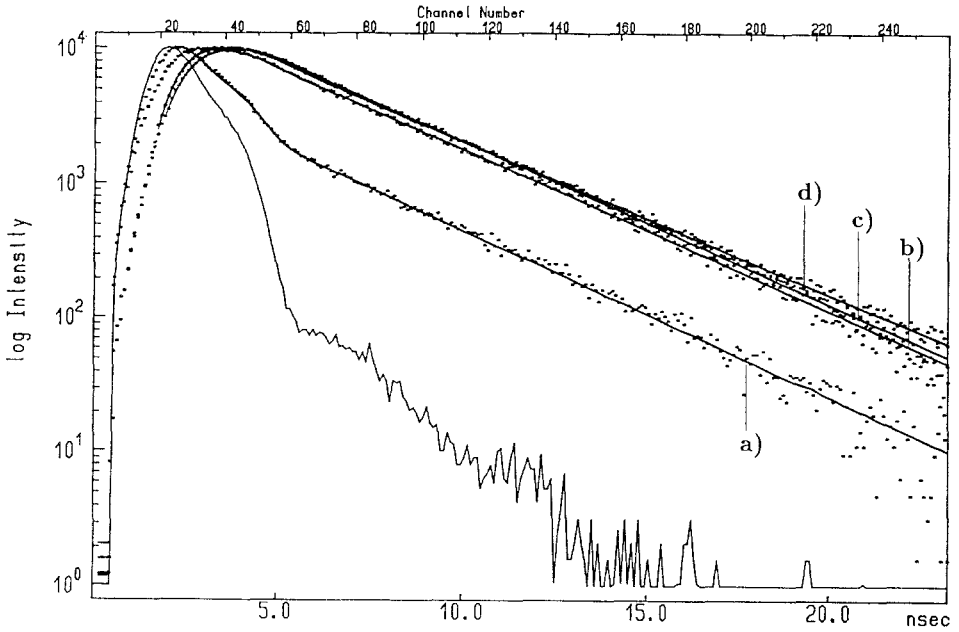

Fig. 5. Overlay representation of dityrosine fluorescence profiles at different emission wavelengths: curves a, b, c, and d are recorded with λ_{ex} = 285 nm and with λ_{em} = 350, 370, 390, and 450 nm, respectively (Table I).

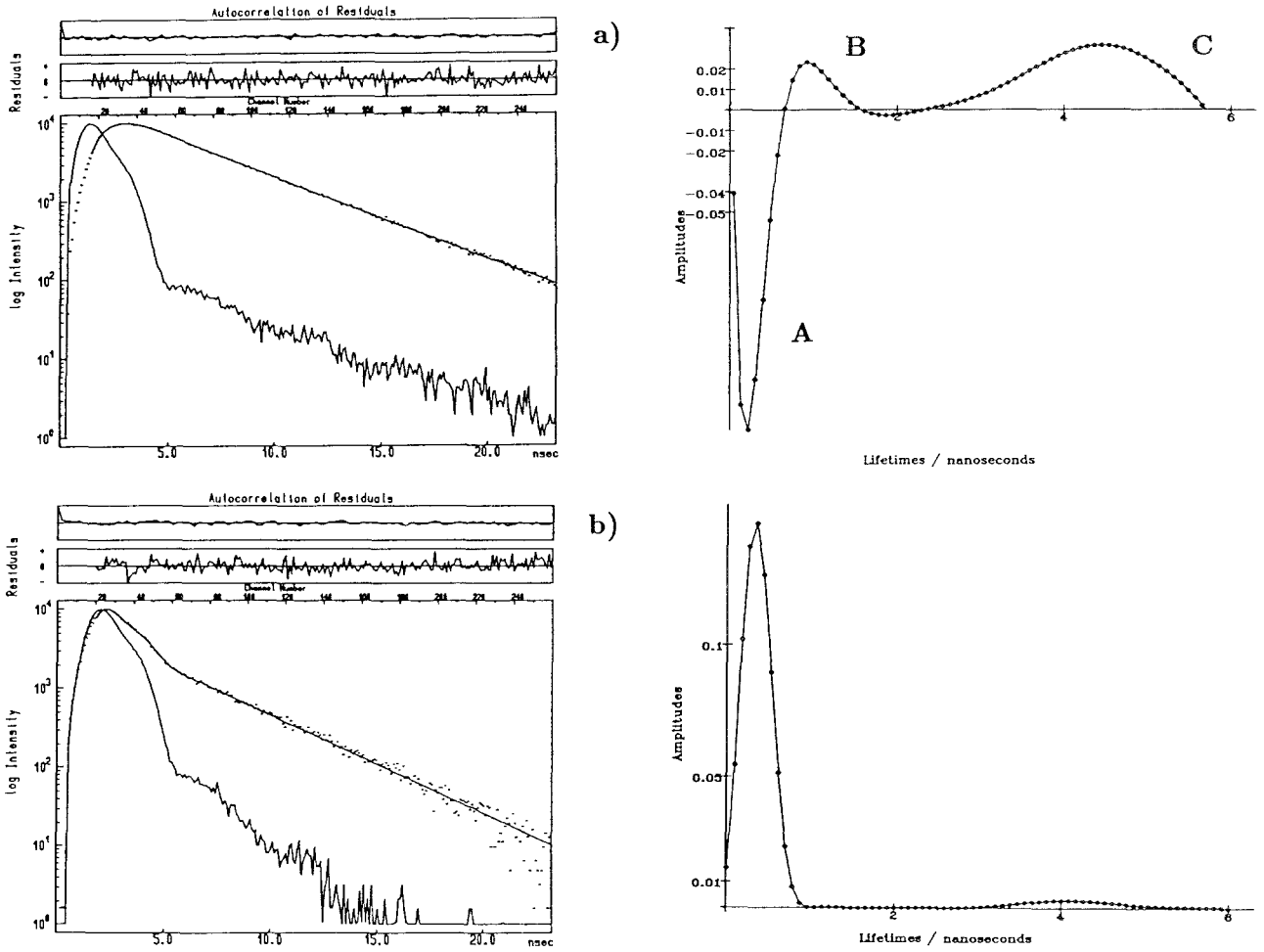

Fig. 6. ESM analysis of experimental dityrosine fluorescence. (a) Successor fluorescence at λ_{em} = 408 nm (counts in the peak channel maximum, 8 × 10^4) with distributions A (negative), B (positive), and C (positive); χ^2 = 0.98. (b) Precursor fluorescence at λ_{em} = 350 nm (counts in the peak channel maximum, 10^4; χ^2 = 1.48); predominant subnanosecond distribution of decay times. See the text for details.

anisotropy started clearly positive but reaches negative values at about 1 ns after the onset of the experiment (starting of rise of laser flash). This negatively going anisotropy is a real effect and is not due to misalignment of the polarizers. We have established for rapidly rotating standard compounds that the g factor is equal to unity and that the anisotropy decays to zero (see, e.g., Refs. 41 and 45). The two polarized intensity decay profiles were globally analyzed in a standard way to yield the short and long correlation times and relative amplitudes [44].

Two exponential terms were needed to fit the pattern adequately: g_1 = 0.29, φ_1 = 0.18 ns; g_2 = −0.01 and an indeterminate value for φ_2 (χ^2 = 0.99). The subnanosecond component of the anisotropy decay (φ_1) in the spectral region of the successor (λ_{em} > 380 nm) closely corresponds to T_1 (Table I) in the precursor and successor transients. T_1 is proposed to represent the time the successor needs to be generated. It can be seen in Fig. 7 that the rise in fluorescence has a similar time course as the decay of the anisotropy. Since φ_1 agrees quite well with the rise time T_1 (Table I), we suggest that electronic dipole reorientation resulting in formally negative values of the anisotropy and formation of the successor species are the same process. The possibility of an associated anisotropy decay in more than one emitting species which can also yield negative values of the anisotropy was not considered in detail because we have not found a more pronounced indication of such a situation.

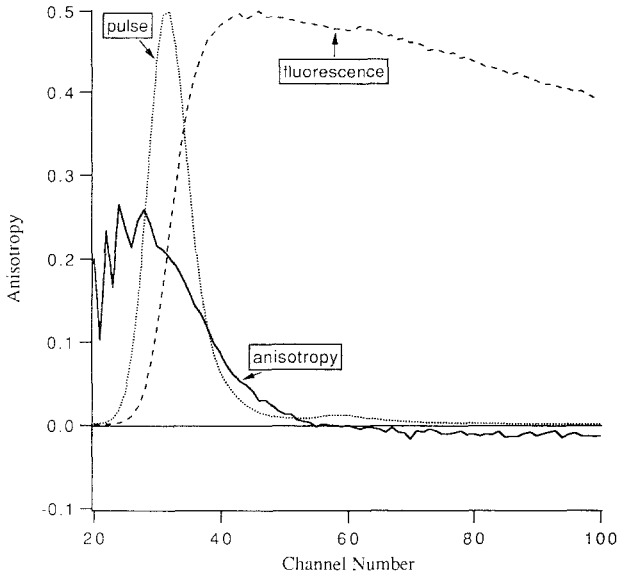

Fig. 7. Time-resolved anisotropy of dityrosine in water (pH 10) recorded at λ_{ex} = 340 nm and λ_{em} = 402 nm with 25.5 ps/channel: g_1 = 0.29, φ_1 = 0.18 ns; g_2 = −0.01; χ^2 = 0.99. For clarity, only the first 100 channels are shown; in addition, the normalized pulse and total fluorescence profiles are given in the same graph.

DISCUSSION

The prominent feature in the optical response of dityrosine is its dual-fluorescence behavior, which — as revealed by time-resolved measurements — shows a pure decay profile [Eq. (4); Fig. 5, curve a; Table I] in the blue edge region near λ_{em} = 350 nm and a typical rise and decay pattern for wavelengths longer than λ_{em} = 380 nm [Fig. 4 and Eq. (3)]. As shown in Fig. 2, the fluorescence emission is shifted by 120 nm in acidic and by 80 nm in alkaline solution, relative to the corresponding absorption band (Figs. 2 and 3). This so-called anomalous Stokes' shift is considered here to be the result of a consecutive excited-state reaction (precursor and successor scheme). The precursor species shows prompt fluorescence after direct ground-state absorption. The successor species is generated in a consecutive excited-state process. The mechanistic aspects of this process are discussed below.

Bridges and co-workers [46] suggested for 2,2′-dihydroxybiphenyl, a substructure of dityrosine, that excited-state deprotonation of a single hydroxyl group accounts for the anomalous Stokes' shift observed for this compound. The photostationary spectra (absorption, excitation, fluorescence) of dityrosine are very similar to those of 2,2′-dihydroxybiphenyl, showing only slight differences in their shapes and intensity maxima. We therefore assume that basic photophysical processes occuring during fluorescence of the two compounds are identical. Since the rise phases in the transient profiles of dityrosine do not depend on the ground-state ionization (lifetimes are practically equal for acidic or basic solutions), we can conclude that the postulated photon-induced proton transfer in acidic medium is an ultra fast process and is not related to the fluorescence subnanosecond rise term. Therefore, the proton transfer from a single hydroxyl-group, either via ground-state ionization and subsequent electronic excitation (basic solution) or by excited-state ionization of the molecule (acidic solution), is essential and results in the same overall fluorescence behavior.

Next we consider the chemical nature of the excited-state reaction. A twisted ground-state configuration is well established for biphenolic compounds [47] and should, therefore, also apply to the ground-state configuration of dityrosine. Both molecules, 2,2′-dihydroxybiphenyl and dityrosine, show a pronounced bathochromic shift in their absorption spectra when varying the pH of the solution from acidic to basic. The relative energetic stabilization in basic medium is due to the formation of the monoanion in the ground state whose oxygen lone-pair electrons tend to participate in the aromatic ring system. Partial electronic delocalization and its tendency to form a conjugated biphenolic system are paralleled by torsional twisting, thus yielding a more planar structure in the ground state as compared to the twisted acidic configuration.

We propose that in the excited state the trend of the monoanion toward additional delocalization and conjugation might be drastically increased. This could again induce planarity by torsional motion. Therefore, the consecutive, low-energy fluorescent state of dityrosine is tentatively identified as a structure consisting of an alternating π system in a quinoid, nonaromatic architecture. The formation of this structure is triggered by (a) configurational mixing between $(n\text{–}\pi)^*$ and $(\pi\text{–}\pi)^*$ states and (b) by the modes of motion along the torsional coordinate of the biphenolic bond. From this point of view, the excited-state reaction exemplified by the subnanosecond rise [and the subnanosecond decay; Eqs. (3) and (4)] is identified as torsional motion. In this context, we believe that intramolecular hydrogen bonding between the phenolate ion and the second (nonionized) phenolic hydroxyl group from a cisoidal geometry as discussed in the work of Bridges *et al.* [46] cannot play an important role in product formation, because 2-hydroxybiphenyl, which is uncapable of forming an intramolecular — O:H–O — interaction, yields the typical long-wave-

length fluorescence too, with a pronounced rise phase practically identical to that of 2,2′-dihydroxybiphenyl (Kungl *et al.*, manuscript in preparation).

However, studies of the dityrosine fluorescence in the calcium metabolizing protein calmodulin revealed no negative preexponential term [34]. The decay of calmodulin photo-crosslinked via dityrosine [49] was best fit by four exponentials with a predominant fluorescence lifetime of 4.4 ns. The lack of a rise term in the calmodulin decay is consistent with results of the natural dityrosine fluorescence in intact yeast spores obtained in our laboratory (Kungl *et al.*, manuscript in preparation). As one would expect, the protein backbone exerts massive constraints on the dynamics and thus on the photophysics of the incorporated dityrosine chromophore, indicating a supression or at least a modification of the reaction in the excited state.

The reaction in the excited state is also manifest in the decay of the fluorescence anisotropy (Fig. 7). The increasing horizontal component of the total intensity decay on a subnanosecond time scale (negative anisotropy) can be explained by a rapid change of the emission dipole moment in the excited state, i.e., the orientation of the dipole moment in the dityrosine successor differs pronouncedly from the orientation of the dipole moment in the initially excited dityrosine precursor. This change in orientation occurs within 180 ps ($=\varphi_1$) in the low-energy spectral region (402 nm), where the successor fluorescence prevails. Thus, the time required for reorientation of the dipole moment is comparable with the rise time T_1 of the dityrosine decay in the respective spectral region ($\lambda_{em} \geqslant 390$ nm; see Table I). Initially, the absorption and emission dipole moments are nearly colinear along the C2–C5 (and C2′–C5′) axis of dityrosine pointing to the hydroxyl groups. We suggest that after excitation, the monoanion rotates to a more planar configuration triggered by a delocalization of the aromatic electrons into both halves of the molecule, leading to a completely different orientation of the emission dipole moment of the successor, now aligned along the biphenolic linkage. The slow course of the anisotropy toward zero ($=\varphi_2$) reflects the restoration of the initial situation before excitation.

Another important result of this study is the pronounced biphasic decay pattern of dityrosine in the low-energy spectral region. This relaxation behavior is quite contrary to the almost monoexponential decay of biphenole fluorescence (Kungl *et al.*, manuscript in preparation). We have to assume that the alanyl side chains of dityrosine are responsible for this finding. This effect is not surprising, as deviations from the monoexponential behavior have been observed for all aromatic amino acids [3–7,11]. In the case of tyrosine and tryptophan, it is now generally accepted that the nonexponentiality of the fluorescence decay is due to distinct charge-transfer quenching routes that arise from some statistically relevant ground-state conformations in which the aromatic chromophore (donor) and the amino or carboxyl group of the alanyl side chain (acceptor) are in close proximity [3,5–7]. In the original "rotamer model," only χ^1 rotamers (conformers of the C_α–C_β dihedral) were taken into account as primary ground-state absorbers. Assuming discrete and noninterconverting fluorescent states, this model could explain nonexponential relaxation. A quite different conclusion has been drawn by Engh *et al.* [48]. From molecular dynamics simulation of tryptophan, they postulated that the χ_2 rotamers are responsible for different charge-transfer quenching rates due to the achirality of the chromophore, whereas the χ_1 conformers interconvert too rapidly to have any influence on the fluorescence decay.

For dityrosine things become even more complicated for the following reasons: (i) the molecule contains two alanyl side chains, whose conformations and state of protonation may influence the fluorescence decay; (ii) the torsional motion of the molecule leading to the excited-state successor is a new feature compared to tyrosine and tryptophan; and (iii) the coplanar quinoid successor state proposed here is the dominant emitter. We suggest a model for the fluorescence kinetics of dityrosine which is a consequence of two emitters in the excited state, the precursor and the successor, respectively. A preliminary assignment can be made: T_1^{-1} refers to the rate of the reaction in the excited state (see above), and T_2^{-1} and T_3^{-1} refer to the rate of deactivation of the precursor and the successor (Table I). The transients of dityrosine are thus dominated by T_1 and T_3, revealing the efficient reaction from the precursor to the successor (T_1) and the dominant emission from the successor (T_3). However, some photons escape from the precursor and are detected with a lifetime T_2, the amplitude of which depends on the spectral range regarded. The varying value of T_2 as well as the trend of its associated preexponential when the wavelength is varied may be due to the fact that other, yet unknown, factors influence the fluorescence lifetime of the precursor, the electronic configuration of which is unknown. The model outlined here has been investigated also with the dityrosine-homologous chromophore *o,o*-bicresole (Kungl *et al.*, manuscript in preparation). The fluorescence transients of dityrosine and of *o,o*-bicresole are very similar indeed. This result, together with the results presented

in the present paper, in our view shows that the "rotamer model" is not needed to explain the time-resolved fluorescence of dityrosine.

Distributional analysis of dityrosine fluorescence revealed three centers in close agreement with the lifetimes found in multiexponential reconvolution (Fig. 6 and Table I). The analysis of negative values in an ESM free fit has become possible with the development of an ESM algorithm in our laboratory [35]. Comparing the results of ESM for areas A, B, and C in Fig. 6a, it appears that the observed "distribution" A, corresponding to the term T_1, is so narrow that we regard this as a discrete exponential. Areas B and C, however, could be real distributions of lifetimes for the two emitting states. The distributions of lifetimes may be due to different microenvironments created by the two alanyl side chains. If these side chains are missing, as is the case for *o,o*-bicresole, the lifetime distributions corresponding to areas B and C are much narrower (data not shown).

ACKNOWLEDGMENTS

This work was financially supported by the Fonds zur Förderung der wissenschaftlichen Forschung, Wien, Austria (Projects P7182 to H.F.K., P7869–PHY to G.L., and P7769–BIO to M.B.), which is gratefully acknowledged. We owe special thanks to Susanne Marinits and Arie van Hoek for technical assistance.

REFERENCES

1. M. G. Badea and L. Brand (1979) *Methods Enzymol.* **61,** 378–425.
2. J. M. Beechem and L. Brand (1985) *Annu. Rev. Biochem.* **54,** 43–71.
3. A. G. Szabo and D. M. Rayner (1980) *J. Am. Chem. Soc.* **102,** 554–563.
4. R. J. Robbins, G. R. Fleming, G. S. Beddard, G. W. Robinson, P. J. Thistlethwaite, and G. J. Woolfe (1980) *J. Am. Chem. Soc.* **102,** 6271–6279.
5. M. C. Chang, J. W. Petrich, D. B. McDonald, and G. R. Fleming (1983) *J. Am. Chem. Soc.* **105,** 3819–3824.
6. P. Gauduchon and P. Wahl (1977) *Biophys. Chem.* **8,** 87–104.
7. W. R. Laws, J. B. Ross, H. R. Wyssbrod, J. M. Beechem, L. Brand, and J. C. Sutherland (1985) *Biochemistry* **25,** 599–607.
8. M. R. Eftink and Z. Wasylewski (1989) *Biochemistry* **28,** 382–391.
9. M. Vincent, J.-C. Brochon, F. Mérola, W. Jordi, and J. Gallay (1988) *Biochemistry* **27,** 8752–8761.
10. N. E. Geactinov and J. Breton (1987) *CRC Crit. Rev. Plant Sci.* **5,** 1–44.
11. D. Creed (1984) *Photochem. Photobiol.* **39,** 537–562.
12. J. W. Petrich, M. C. Chang, D. B. McDonald, and G. R. Fleming (1983) *J. Am. Chem. Soc.* **105,** 3824–3832.
13. E. Gudgin, R. Lopez-Delgado, and W. R. Ware (1981) *Can. J. Chem.* **59,** 1037–1044.
14. T. R. Rizzo, Y. D. Park, and D. H. Levy (1986) *J. Chem. Phys.* **85,** 6945–6951.
15. J. Sipior and M. Sulkes (1988) *J Chem. Phys.* **88,** 6146–6156.
16. D. R. James and W. R. Ware (1985) *Chem. Phys. Lett.* **120,** 455–459.
17. D. R. James and W. R. Ware (1986) *Chem. Phys. Lett.* **126,** 7–11.
18. B. D. Wagner, D. R. James, and W. R. Ware (1987) *Chem. Phys. Lett.* **138,** 181–184.
19. J. R. Alcala, E. Gratton, and F. G. Prendergast (1987) *Biophys. J.* **51,** 587–596, 597–604, 925–936.
20. I. Gryczynski, M. Eftink, and J. R. Lakowicz (1988) *Biochim. Biophys. Acta* **954,** 244–252.
21. J. Skilling and S. F. Gull (1985) in C. R. Smith and W. T. Grandy (Eds.), *Maximum-Entropy and Bayesian Methods in Inverse Problems,* D. Reidel, Dordrecht/Boston/Lancaster, pp. 83–133.
22. A. K. Livesey and J.-C. Brochon (1987) *Biophys. J.* **52,** 693–706.
23. F. Mérola, R. Rigler, A. Holmgren, and J.-C. Brochon (1989) *Biochemistry* **28,** 3383–3398.
24. A. J. Gross and I. Sizer (1959) *J. Biol. Chem.* **234,** 1611–1614.
25. P. Briza, G. Winkler, H. Kalchhauser, and M. Breitenbach (1986) *J. Biol. Chem.* **261,** 4288–4294.
26. S. O. Andersen (1964) *Biochim. Biophys. Acta* **93,** 213–215.
27. D. J. Raven, C. Earland, and M. Little (1971) *Biochim. Biophys. Acta* **251,** 96–99.
28. N. K. Pandey and A. I. Aronson (1979) *J. Bacteriol.* **137,** 1208–1218.
29. C. A. Foerder and B. M. Shapiro (1977) *Proc. Natl. Acad. Sci. USA* **74,** 4214–4218.
30. P. Briza, A. Ellinger, G. Winkler, and M. Breitenbach (1988) *J. Biol. Chem.* **263,** 11569–11574.
31. K. J. Deeg, L. Katsikas, and W. Schnabel (1987) *Int. J. Radiat. Biol. Relat. Stud. Phys. Chem. Med.* **51,** 527–540. D. A. Malencik and S. R. Andersen (1987) *Biochemistry* **26,** 695–704. G. Boguta and A. Dancewicz (1985) *Nukleonika* **30,** 47–53.
32. R. Amado, R. Aeschbach, and H. Neuko (1984) *Methods Enzymol.* **107,** 377–388.
33. T. Deits, M. Farrance, E. S. Kay, L. Medill, E. E. Turner, P. J. Weidmann, and B. M. Shapiro (1984) *J. Biol. Chem.* **259,** 13525–13535.
34. E. W. Small and S. R. Anderson (1988) *Biochemistry* **27,** 419–428.
35. G. Landl, T. Langthaler, H. W. Engl, and H. F. Kauffmann (1991) *J. Comp. Phys.* **95,** 1–28.
36. S. O. Andersen (1963) *Biochim. Biophys. Acta* **69,** 249–262.
37. D. V. O'Connor and D. Phillips (1984) *Time-Correlated Single Photon Counting,* Academic Press, London.
38. A. Grinvald and I. Z. Steinberg (1974) *Anal. Biochem.* **59,** 583–598.
39. M. Al-Baali and R. Fletcher (1985) *J. Operat. Res. Soc.* **36,** 405–415. R. Fletcher and C. Xu (1987) *IMA J. Num. Anal.* **7,** 371–380.
40. A. van Hoek, K. Vos, and A. J. W. G. Visser (1987) *IEEE J. Quant. Electr.* **QE-23,** 1812–1820.
41. A. J. W. G. Visser, K. Vos, A. van Hoek, and J. S. Santema (1988) *J. Phys. Chem.* **92,** 759–765.
42. A. van Hoek and A. J. W. G. Visser (1981) *Rev. Sci. Instrum.* **52,** 1199–1205.
43. A. J. W. G. Visser, T. Kulinski, and A. van Hoek (1988) *J. Mol. Struct.* **175,** 111–116.
44. K. Vos, A. van Hoek, and A. J. W. G. Visser (1987) *Eur. J. Biochem.* **165,** 55–63.
45. R. Leenders, P. Bastiens, R. Lunsche, A. van Hoek, and A. J. W. G. Visser (1990) *Chem. Phys. Lett.* **165,** 315–323.

46. J. W. Bridges, P. J. Creaven, and R. T. Williams (1965) *Biochem. J.* **96,** 872–878.
47. W. F. Baitinger, P. R. Schleyer, and K. Mislow (1965) *J. Am. Chem. Soc.* **87,** 3168–3173. M. Remko and J. Polcin (1980) *Z. Phys. Chem.* **120,** 1–8.
48. R. A. Engh, L. X.-Q. Chen, and G. R. Fleming (1986) *Chem. Phys. Lett.* **126,** 365–372.
49. D. A. Malencik and S. R. Anderson (1987) *Biochemistry* **26,** 695–704.